Geophysical Research Letters

RESEARCH LETTER
10.1029/2023GL102984

Key Points:

- The 2021 winter tornado outbreak left significant linear scars on Arkansas aquert farmland observed from Moderate Resolution Imaging Spectroradiometer (MODIS) shortwave infrared (SWIR) channels
- The scars are unrecognizable on MODIS visible and near-infrared channels due to the coarse resolution and rare vegetation cover in winter
- SWIR provides a fast assessment of tornado track as topmost layer is removed by suction vortices and wetter underlying soil is exposed

Supporting Information:

Supporting Information may be found in the online version of this article.

Correspondence to:

J. Wang and Y. Lin,
jingyu.wang@nie.edu.sg;
yunlin@ucla.edu

Citation:

Wang, J., Lin, Y., McFarquhar, G. M., Park, E., Gu, Y., Su, Q., et al. (2023). Soil moisture observations from shortwave infrared channels reveal tornado tracks: A case in 10–11 December 2021 tornado outbreak. *Geophysical Research Letters*, *50*, e2023GL102984. https://doi.org/10.1029/2023GL102984

Received 7 NOV 2022
Accepted 23 FEB 2023

Author Contributions:

Conceptualization: Jingyu Wang, Yun Lin
Data curation: Jingyu Wang, Yun Lin, Greg M. McFarquhar, Qiong Su, Tianhao Zhang
Formal analysis: Jingyu Wang
Funding acquisition: Jingyu Wang, Rong Fu
Investigation: Jingyu Wang, Yun Lin
Methodology: Jingyu Wang, Yun Lin, Greg M. McFarquhar, Edward Park, Kee Wei Lee

Soil Moisture Observations From Shortwave Infrared Channels Reveal Tornado Tracks: A Case in 10–11 December 2021 Tornado Outbreak

Jingyu Wang[1], Yun Lin[2], Greg M. McFarquhar[3], Edward Park[1,4], Yu Gu[2], Qiong Su[5], Rong Fu[2], Kee Wei Lee[6], and Tianhao Zhang[2]

[1]National Institute of Education, Nanyang Technological University, Singapore, Singapore, [2]Joint Institute for Regional Earth System Science and Engineering, Department of Atmospheric and Oceanic Sciences, University of California, Los Angeles, Los Angeles, CA, USA, [3]School of Meteorology, Cooperative Institute for Severe and High-Impact Weather Research and Operations, University of Oklahoma, Norman, OK, USA, [4]Earth Observatory of Singapore, Nanyang Technological University, Singapore, Singapore, [5]Department of Agricultural Sciences, Clemson University, Clemson, SC, USA, [6]Asian School of the Environment, Nanyang Technological University, Singapore, Singapore

Abstract Satellite-based post-tornado assessments have been widely used for the detection of tornado tracks, which heavily relies on the identification of vegetation changes through observations at visible and near-infrared channels. During the deadly 10–11 December 2021 tornado outbreak, a series of violent tornadoes first touched down over northeastern Arkansas, an area dominated by cropland with rare vegetation coverage in winter. Through the examination of Moderate Resolution Imaging Spectroradiometer multi-spectral observations, this study reveals significant scars on shortwave infrared channels over this region, but none are captured by visible and near-infrared channels. The dominant soil type is aquert (one of vertisols), whose high clay content well preserves the severe changes in soil structure during the tornado passage, when the topmost soil layer was removed and underlying soil with higher moisture content was exposed to the air. This study suggests a quick post-tornado assessment method over less vegetated area by using shortwave infrared channels.

Plain Language Summary This study showcases an application of using Moderate Resolution Imaging Spectroradiometer (MODIS) data to detect tornado damage tracks over northeastern Arkansas after the deadly 10–11 December 2021 tornado outbreak. The special soil type with rich clay content well retains the tornado scars, whose moisture content is higher than the surrounding area, causing significant signals on MODIS shortwave infrared channels. Although coarse in spatial resolution, MODIS's rapid revisit cycle and minimal latency in data availability make it an ideal platform for the post-tornado assessment over the winter farmland, when the vegetation coverage is low, thus the conventional vegetation-based tornado track detection does not work well.

1. Introduction

Tornadoes are one of the most destructive extreme weather hazards in the United States, causing significant property damage and casualties every year (Changnon, 2009). Identifying the complete tornado damage track is crucial for the post-tornado assessment of tornado intensity, path, extent, and touch down location, which provides observational ground-truth to improve the understanding and evaluate numerical simulations of tornadogenesis, maintenance, and dissipation processes. In addition to human witness reports, radar observations, and labor-intensive ground surveys, the improved remote sensing technology since the late 1990s has promoted tornado track assessments via satellite imagery (Jedlovec et al., 2006; Skow & Cogil, 2017; Yuan et al., 2002), which continue to this day. This further extends to analysis of remote sensing data collected by Unmanned Aerial Systems (Wagner et al., 2019) to perform damage surveys.

The usage of remotely sensed imagery to detect tornado damage tracks is based on the physical principle that the tornado-associated winds will disturb the physical characteristics of the surface, thus resulting in abrupt changes in reflective properties at certain wavelengths detected by remote sensors. The altered spectral signature can be captured by comparing the imagery before and after the event to locate the tornado track (Jedlovec et al., 2006). Among different remote sensing wavelengths, visible (0.4–0.7 μm; represented by the red channel) and near-infrared channels (NIR; 0.75–1.35 μm) have been most widely used for tornado damage detection because

Project Administration: Jingyu Wang, Yun Lin, Yu Gu, Rong Fu
Resources: Jingyu Wang, Yun Lin, Qiong Su, Kee Wei Lee
Software: Jingyu Wang
Supervision: Jingyu Wang, Edward Park, Yu Gu, Rong Fu
Validation: Jingyu Wang, Yun Lin, Greg M. McFarquhar, Edward Park, Qiong Su
Visualization: Jingyu Wang
Writing – original draft: Jingyu Wang, Yun Lin
Writing – review & editing: Jingyu Wang, Yun Lin, Greg M. McFarquhar, Edward Park, Yu Gu, Qiong Su, Tianhao Zhang

(a) healthy vegetation tends to strongly absorb at visible wavelengths and reflect more energy at near-infrared wavelengths to enhance photosynthesis (Kingfield & de Beurs, 2017); (b) the underlying soil background has a distinct reflective pattern relative to the vegetation canopy which is generally more reflective in visible channels but less reflective in near-infrared channels (Cohen & Goward, 2004); and (c) the vegetation damaged by destructive winds will resemble the soil background, presenting a spectral signature opposite to that of healthy vegetation. As a result, many previous studies have employed the Normalized Difference Vegetation Index (NDVI; Rouse et al., 1974; defined as [NIR − red]/[NIR + red]) to identify the damages of tornadoes (e.g., Kingfield & de Beurs, 2017; Molthan et al., 2014; Yuan et al., 2002), hurricanes (Ramsey et al., 1997; Wang et al., 2010), hailstorms (e.g., Bell & Molthan, 2016; Gallo et al., 2012; Klimowski et al., 1998), and thunderstorm winds (e.g., Szwagrzyk et al., 2017).

Similarly, different variants of vegetation indices have been examined for severe weather damage, such as the Leaf Area Index (LAI; Aosier & Kaneko, 2007) and the enhanced vegetation index (EVI; Wang et al., 2010). The assessment method based on reduced vegetation indices has shown potential to capture damage patterns over well-vegetated areas like cropland and forest. However, the scar patterns are not as obvious or totally disappear on other types of land use, for example, grassland and bare soil where there is little vegetation coverage (Jedlovec et al., 2006). Later, Wang et al. (2010) extended the spectral range to shortwave infrared (SWIR; 1.5–2.5 μm) and found that the Normalized Difference Infrared Index (NDII; defined as [NIR − SWIR]/[NIR + SWIR]) shows higher disturbance detection accuracy than NDVI and other conventional vegetation indices. Thus, the Landsat Thematic Mapper (TM) channel 4 (0.85 μm) and channel 5 (1.65 μm) were adopted to assess the post-hurricane forest damage, which later was applied for the track detection of 1984 Ivanovo tornado outbreak in Russia (Chernokulsky & Shikhov, 2018). The rationale of using NDII for damage detection is that the NIR reflectance is positively correlated with plant chlorophyll content, while the SWIR has an inverse relationship with plant moisture content. Compared to plant moisture, SWIR is more indicative of soil moisture content as many soil types are highly reflective in this spectral range and wetter soil tends to be less reflective compared to dry soil (Kingfield & de Beurs, 2017).

In this study, using Moderate Resolution Imaging Spectroradiometer (MODIS) SWIR channels, we found multiple significant soil moisture scars on Arkansas aquert farmland after the 10–11 December 2021 tornado outbreak, one of which is indicative of a tornado track. Other scars may be caused by gusty winds associated with the storm systems. However, these signatures were absent from visible and NIR channels that are conventionally used for tornado track detection because of the rare vegetation coverage in winter. This is a joint result of (a) the uniform land use type of cropland with bare soil exposed to the air, (b) the dominant soil type of aquert whose high clay content can well preserve the structure change caused by tornadoes, and (c) the higher soil moisture content in the deeper layer which can be captured by SWIR channels because the topmost, relatively dry soil is removed by the suction vortices from tornadoes.

By utilizing sharp changes in SWIR channels where vertical soil moisture structure is substantially disturbed by tornadoes, this study provides a novel approach to detect tornado tracks during winter when the vegetation coverage is rare, and conventional detection methods based on the destruction of vegetation are not appropriate. Moreover, this study also aims to explore the possibility of identifying the tornado damage at earlier stages of the outbreak over less populated agricultural land in a quantitative way. Last and most importantly, with soil serving as a good medium to record the scale and severity of a tornadic vortex, the near-surface characteristics of tornadoes that are inaccessible through in-situ measurements can be better understood.

2. Data and Methods

2.1. Case Description

During the deadliest tornado outbreak on record in December, a series of violent, prolonged tornadoes swept through multiple Midwest states from the evening of 10 December to the early morning of 11 December 2021. A total of 102 tornadoes were reported within 24 hr starting from 1200 UTC 10 December 2021 according to the filtered storm records by the National Oceanic and Atmospheric Administration (NOAA) Storm Prediction Center (SPC, available at https://www.spc.noaa.gov/climo/reports/211210_rpts.html). As shown in Figure 1a, the majority of tornado reports during that day were spawned by the violent, long-tracked tornado (EF4) extending from northeastern Arkansas to western Kentucky. The supercell that produced the most devastating western Kentucky tornado was initiated over Arkadelphia around 20:00 UTC, 10 December, then at 00:40 UTC, it made

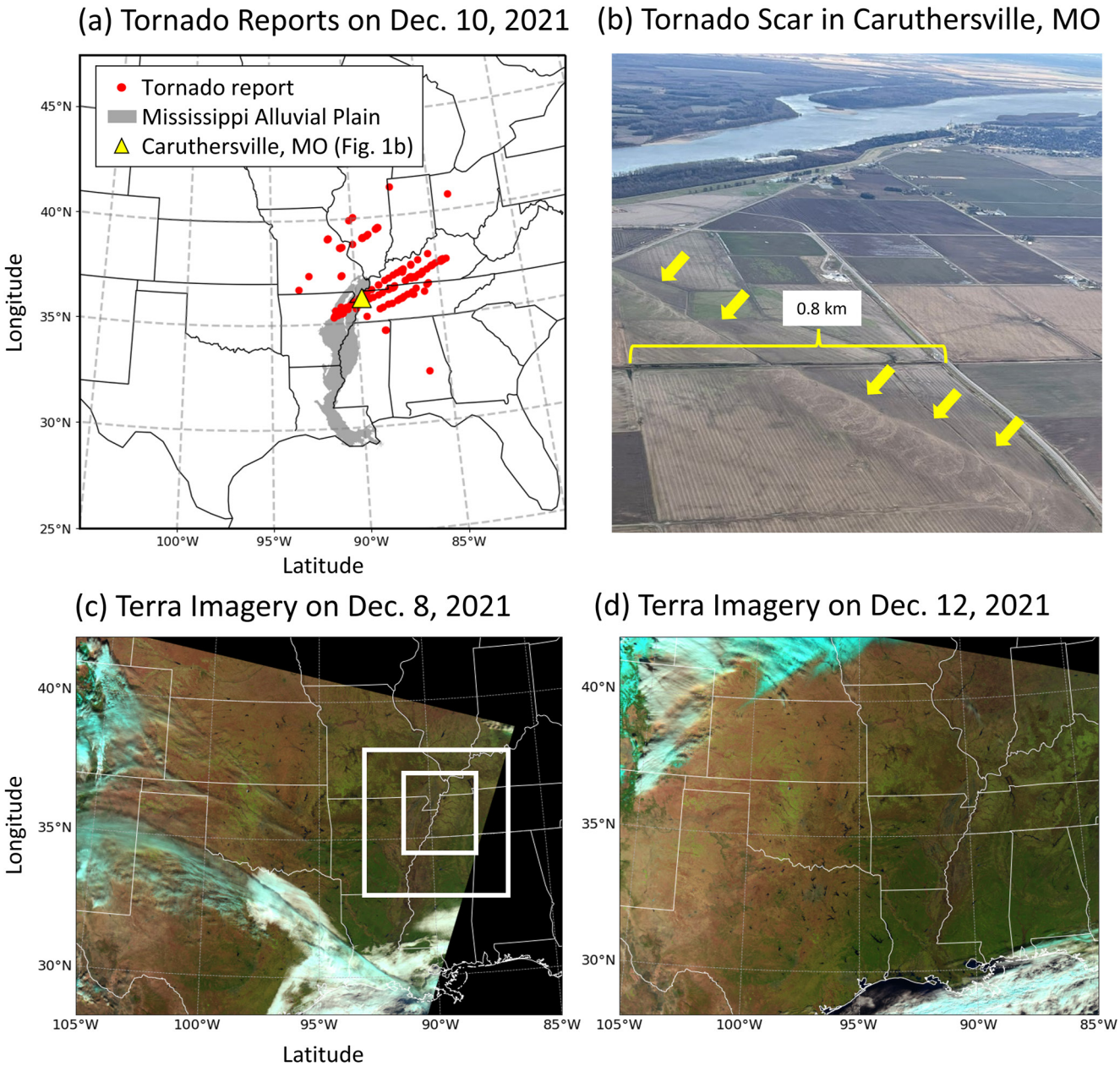

Figure 1. (a) The filtered tornado reports (red dots) obtained from National Oceanic and Atmospheric Administration Storm Prediction Center archive (https://www.spc.noaa.gov/climo/reports/211210_rpts.html), where the Mississippi Alluvial Plain is shaded gray. (b) The aerial photo of a tornado scar (indicated by yellow arrows) over Caruthersville, Missouri. The location is denoted as a yellow triangle on panel (a). Photo curtesy of Tab Wildy (https://twitter.com/twildy), retrieved from https://twitter.com/twildy/status/1469847790394261505/photo/1 (accessed on 20 July 2022). Natural color imagery captured by Terra satellite on (c) 8 December and (d) 12 December 2011. There are two white boxes on (c), where the inner box (34.5°–37.5°N, 91.5°–88.5°W) encloses the region for the examination of tornado damage track and the outer box (33°–38°N, 93°–89°W) is for the background comparison.

the first EF0 tornado touch-down over western Poinsett County. As the supercell propagated northeastward while maintaining its high-end rotational vorticity signature, larger and more intense tornadoes were produced along the track over Missouri, Tennessee and Kentucky (Moriarty et al., 2021). In addition to human spotter and radar observations, aerial-based detection confirms the passage of tornado (Figure 1b) by showing the evidence of striations on cropland, where the topmost soil layer was removed by suction vortices of the tornado. An outer domain (33°–38°N, 93°–89°W) is selected to roughly enclose the region raked by tornadoes and examine the overall spatial patterns, within which an inner domain (34.5°–37.5°N, 91.5°–88.5°W) is refined to conduct statistical analyses.

2.2. Characteristics of Underlying Surface

Over northeastern Arkansas where the western Kentucky tornado made its first touch-down, the dominant land use type is cropland, with a small portion of cropland mixed with pasture and forest (Figure S1a in Supporting Information S1). The 2021 crop inventory (Figure S1b in Supporting Information S1) shows the major crop types are corn (harvested in late August to early September), cotton (harvested from November to early December), and rice, sorghum, and soybean (harvested in September). Therefore, surface vegetation coverage was low during the tornado outbreak. Although located within the Mississippi Alluvial Plain, there are two distinct soil types over this region, alfisols (udalfs and aqualfs; Figure S1c in Supporting Information S1) and vertisol (aquerts; Figure S1d in Supporting Information S1). In general, compared with clayey vertisols (Coulombe et al., 1996), alfisols contain more silt and sand (Pathak et al., 2013a, 2013b). The contrast in composition between the two types of soil is more significant over northeastern Arkansas. According to the detailed soil survey geographic database (Figure S1e in Supporting Information S1; SSS, 2022), the major subtype of vertisols over the inner study domain is Sharkey soil, which has a clay content ≥60% to a depth of 250 cm (Han et al., 2007; Pettry & Switzer, 1998). While in the neighboring alfisols, Tichnor is the dominant subtype, whose clay content is merely 16% in the top 50 cm. The huge contrast in soil composition gives the two types of soil different physical characteristics in (a) speed of recovery to the change of disturbance in surface layer texture, and (b) infiltration rate and moisture holding capacity (Kanwar, 1982), which further shapes their distinctive vertical soil moisture profiles. The clay-rich vertisols have high plasticity when wet, therefore the change in surface layer texture can be well preserved. However, for alfisols, their low clay content makes such changes relatively easy to recover by wind and precipitation. Meanwhile, clayey soils have higher field capacity (40%) than sandy and silty soils (15%–30%, Singh & Su, 2022), thus vertisols usually have higher water content than alfisols when they are saturated. The contrast in these features between the two types of soil results in different reflective signatures after tornado passage, which is revealed in Section 3.1 and explained in Section 3.2.

2.3. MODIS Observation and Remote Sensing Indices

MODIS is a key instrument onboard the Terra and Aqua satellites launched in 1999 and 2002 respectively. Although coarse in spatial resolution (250 m in channels 1–2, 500 m in channels 3–7), MODIS's rapid daily update cycle with minimal data latency of a few hours makes it an ideal observation for the quick assessment of the change in land, cloud, aerosol properties, as well as for tornado damage path assessment. As suggested by Molthan et al. (2011), MODIS imagery is capable of detecting tornadoes with path lengths longer than its pixel size. However, MODIS-based tornado damage track detection heavily relies on the sharp changes in the red visible channel where vegetation has been destroyed by tornadoes. Similarly, the application of tornado track detection during the 10–11 December 2021 outbreak has been documented through the manual screening of natural color imagery (https://www.universetoday.com/153716/the-recent-killer-tornados-track-is-visible-from-space/, accessed on 1 February 2022; https://www.nasa.gov/feature/esnt/2021/nasa-satellite-data-used-to-assess-tornado-damage-understand-storms, accessed on 30 December 2021), which only indicates the damage track over western Kentucky where the most severe long-track EF4 tornado occurred. Instead of qualitative examination of tornado damage track over the region with confirmed reports, this study explores the possibility of tornado track identification at earlier stages of the outbreak over the less populated agricultural land in a quantitative way. Through the examination of MODIS's multispectral observations, we unravel some overlooked reflective signatures on the vast homogeneous cropland with distinctive soil types, providing more evidence for the accurate assessment of the tornado touch-down location.

Details of MODIS bandwidths are available in Table S1 in Supporting Information S1, and its different channels are named in the convention of MX, where X denotes the order of MODIS channels. Therefore, the natural color image is composed using the combination of R: M1, G: M4, B: M3, and the NDVI is calculated as $(M2 - M1)/(M2 + M1)$.

In addition to the visible and NIR channels that are sensitive to the change in vegetation coverage, Yue et al. (2019) and Tian et al. (2021) suggest that SWIR channels (SWIR1: 1,550–1,750 nm, SWIR2: 2,100–2,300 nm; Multispectral Instrument on-board SENTINEL-2) are inversely correlated with soil moisture content. Regarding the reflection decreasing trend with increasing soil moisture, SWIR2 shows a significantly faster rate than SWIR1. Therefore, a series of soil moisture indices were developed (Yue et al., 2019). By substituting SWIR1

with M6 (1,628–1,652 nm) and SWIR2 with M7 (2,105–2,155 nm), the normalized shortwave-infrared difference soil moisture indices (NSDSIs) are written as:

$$\text{NSDSI1} = (\text{M6} - \text{M7})/\text{M6}, \quad (1)$$

$$\text{NSDSI2} = (\text{M6} - \text{M7})/\text{M7}, \quad (2)$$

$$\text{NSDSI3} = (\text{M6} - \text{M7})/(\text{M6} + \text{M7}), \quad (3)$$

where higher NSDSI values corresponds to higher soil moisture content.

The MODIS data collected onboard Terra on 8 and 12 December 2021 are analyzed for the comparison of surface conditions "before" and "after" tornado passage. As shown in Figures 1c and 1d, those two dates are most adjacent to the 10–11 December tornado outbreak with clear sky over the study region.

The MODIS data are level 1B calibrated radiances (MOD02HKM) downloaded from the National Aeronautics and Space Administration (NASA) Level-1 and Atmosphere Archive & Distribution System Distributed Active Archive Center (LAADS DAAC; MODIS Characterization Support Team, 2017). The native 500 m resolution is used for all channels, and the data on both 8 and 12 December are remapped to an equal angle latitude-longitude grid with grid spacing of 0.005° through nearest interpolation to facilitate the calculation of changes in NDVI and NSDSIs.

3. Results

3.1. The Soil Moisture Scar Observed by MODIS Shortwave Infrared Channels

All the indices are constructed for both days, and the changes are calculated by subtracting 8 December from 12 December. For NDVI, over the entire outer domain, there is an overall increasing trend after the tornado outbreak (Figure 2a). The most prominent decrease is observed over the water bodies of the Upper Mississippi River, Kentucky Lake, Lake Barkley, and Arkansas River, which likely reflects the change in water depth between the two dates (Cho et al., 2008). By zooming into the inner domain, there are scattered pixels with reduced NDVI values over northeastern Arkansas, the Missouri Bootheel, and western Kentucky, which are probably indicative of tornado damage. By highlighting the pixels with the most significant NDVI decrease (below 2nd percentile of the entire population) in Figure 2b, some overlaps are found between these anomalies and tornado reports, but no persistent linear NDVI scars are observed. In addition to the point observations, the two-dimensional tornado tracks from the NOAA Damage Assessment Toolkit (DAT) are overlaid. It is noteworthy that there are spatial mismatches between the point-based reports and linear tracks with 20 out of 61 reports lying outside of the tornado damage tracks within the outer domain. For example, the tornado tracks skewed southward compared to the reports over the northeast corner of the domain. The inconsistency between the two data sets also necessitates the exploration of new tornado damage track detection techniques as proposed in this study. To account for the uncertainty in reported tornado locations, when mapping the tornado reports on the MODIS grid using the nearest neighbor method, their locations are aggregated by one pixel (forming a 3 by 3 window) to account for the possible spatial uncertainty in tornado reports.

By comparing the binarized images between the NDVI anomaly (pixels with significant decrease are marked with 1; the rest are marked with 0) and the rasterized tornado reports (1 for tornado location and 0 for null), a total of 3 matching pixels (i.e., the pixels with significant change from post-event to pre-event that collocate with tornado reports) are identified with a spatial correlation (Pearson product-moment correlation coefficient) of −0.002. From the density scatter plots (Figures 2c and 2d), pixels within the inner domain show a distribution consistent with the outer domain, where the ratio of 12–8 December slightly increases from 1.09 to 1.11, while the correlation coefficients between the two days are also comparable (0.89 vs. 0.87). Therefore, the change in NDVI derived from MODIS is incapable of the quantitative detection of tornado damage track, especially over the homogeneous cropland, because (a) the vegetation coverage is greatly reduced in winter and (b) the coarse resolution image is insufficient to capture the vegetation changes at finer scale.

Following Equation 1, the NSDSI1 values are compared between the two observations in Figure 3. Different from the overall increasing trend in NDVI (Figure 2a), a reduction of domain average post-event over pre-event ratio from 1.09 (Figure 2c) to 0.99 (Figure 3c) is observed over the majority of the study region (Figure 3a) except

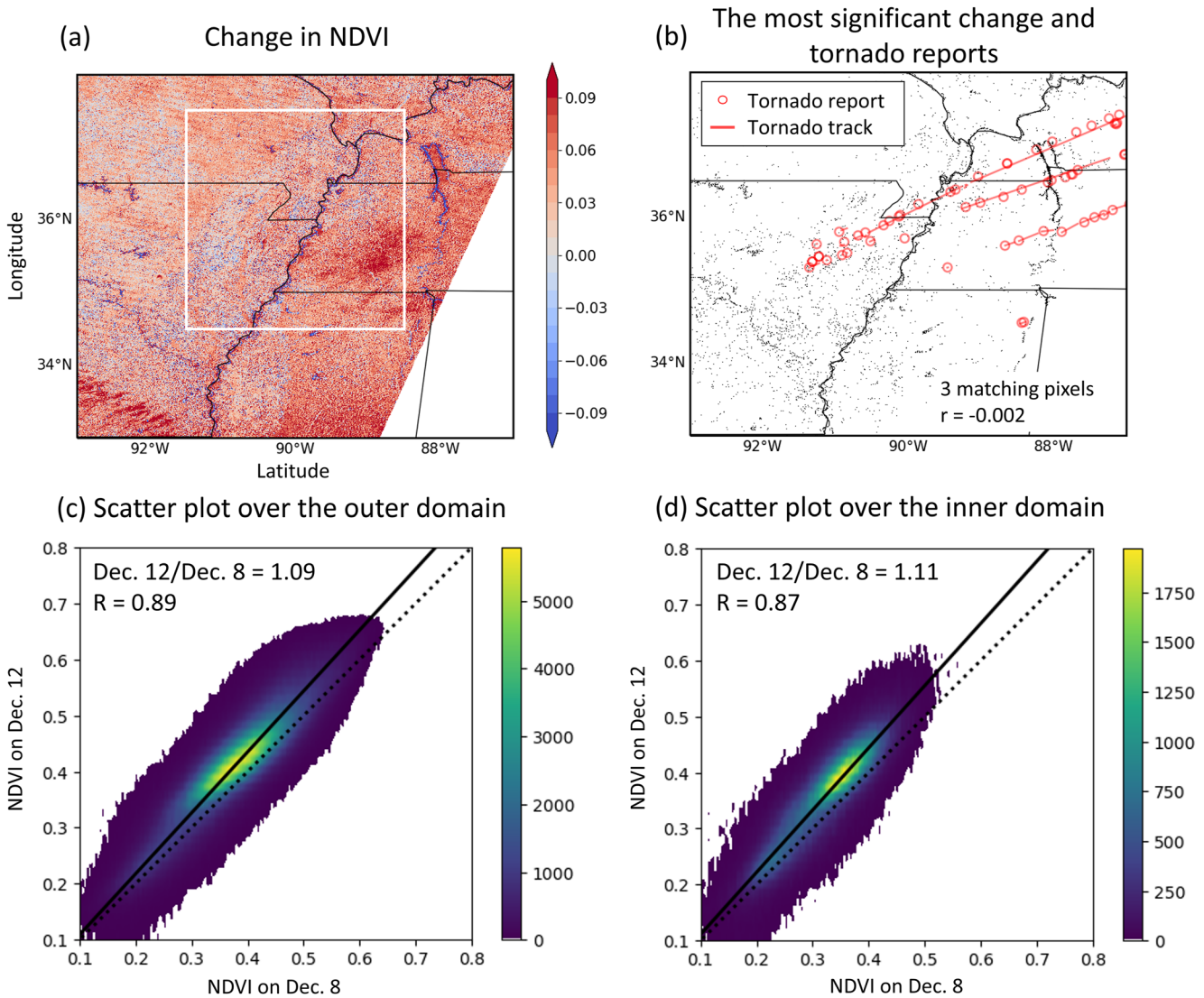

Figure 2. (a) The changes in NDVI (12 December minus 8 December) over the outer domain as denoted in Figure 1c, where the white box indicates the inner domain. (b) Pixels with the most significant decrease (below 2nd percentile of the entire population) are marked with black, overlaid by the tornado reports (red circles). The density scatter plots over (c) the outer domain and (d) the inner domain.

for the cropland on alfisols and vertisols over northeastern Arkansas and northwestern Mississippi. Over these regions, an absolute increase of more than 0.15 in NSDSI1 value is found, indicates a surge in soil moisture after the tornado outbreak. Statistically, 15 matching pixels and a spatial correlation of 0.005 is found between the NSDSI1 anomaly and tornado reports. The comparison in population between the two domains (Figures 3c and 3d) confirms this contrast, where the ratio of 12–8 December shifts from 0.99 (decreasing in outer domain) to 1.02 (increasing in inner domain), and the correlation coefficient notably decreases (0.69 vs. 0.59).

Through the examination of the locations with the most significant NSDSI1 increase (Figure 3b), several clusters are found mostly over the cropland with vertisols coverage. One of them shows a prominent linear pattern which well overlaps with a tornado report to the west of Osceola (35.71°N, 90.05°W, highlighted in blue in Figure 3b; https://www.spc.noaa.gov/climo/reports/211210_rpts.html). The coincidence between the linear NSDSI1 scar (surplus soil moisture) and the confirmed tornado report implies the physical disturbance of soil structure as depicted in Figure 1b may leave a notable signature on surface reflective properties, which can be captured by MODIS SWIR channels.

Such coincidence is also observed by using NSDSI2 (Figure S2 in Supporting Information S1) and NSDSI3 (Figure S3 in Supporting Information S1). To facilitate comparison, the significant changes and tornado reports are summarized for NDVI and NSDSIs in Figure 4. Through visual inspection, the linear scar with significant

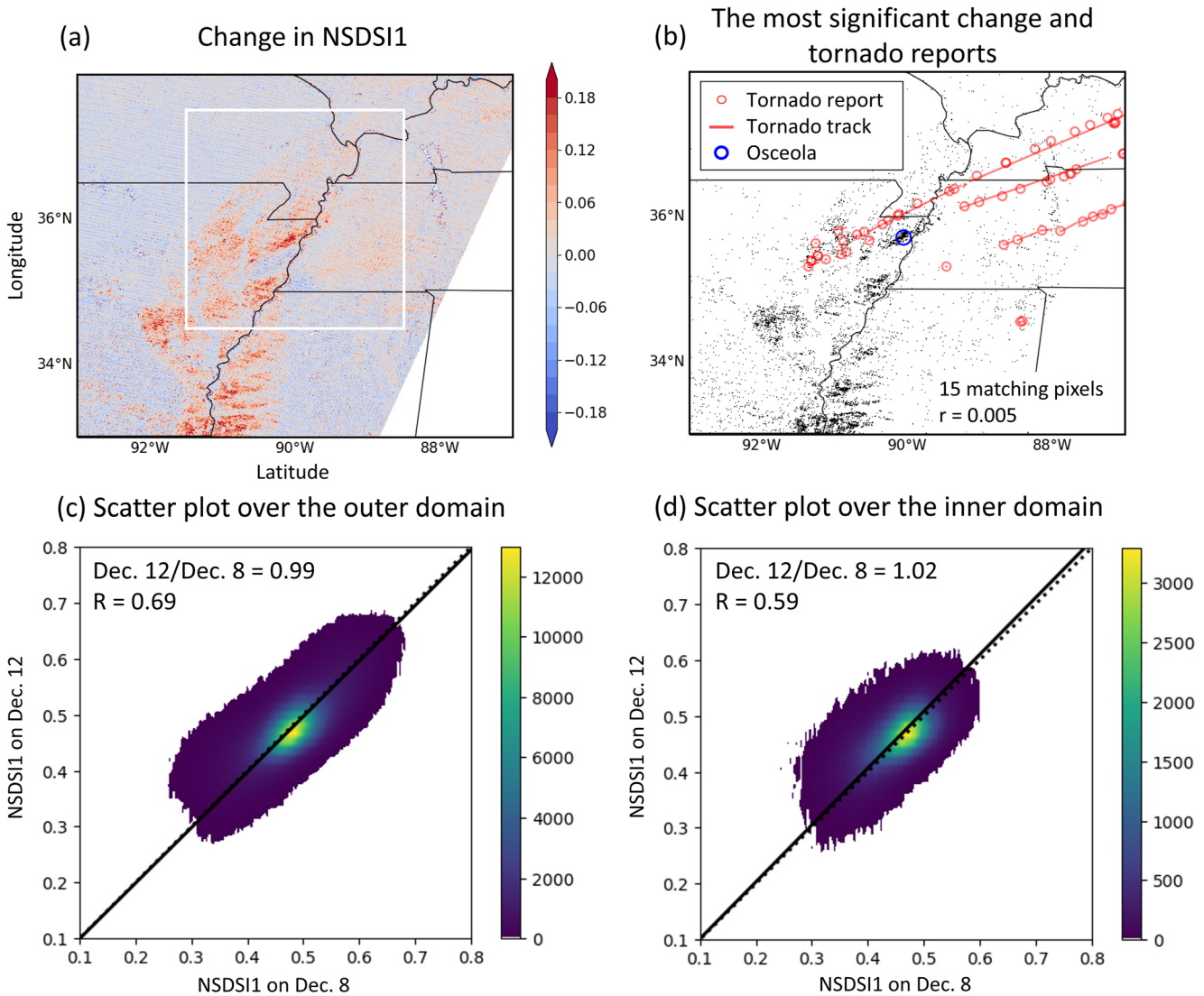

Figure 3. Same as Figure 2, but for the index of NSDSI1, and the significance has been changed to pixels with NSDSI1 value above 98th percentile in (b).

surge in soil moisture is observed for all NSDSIs, which is absent from NDVI. Statistically, more matching pixels (7–15 vs. 3) and higher spatial correlations (0.002–0.005 vs. −0.002) are found between tornado reports and NSDSIs than NDVI. Similar as the matching between the pixels with significant change and the tornado reports, the statistics of intersection between those pixels and tornado tracks are provided in Table S2 in Supporting Information S1. Although the contrast between NDVI and NSDSIs is not as prominent as that of point-based reports because of the inclusion of vast non-vertisols areas, it is still supportive of the finding that soil moisture could return stronger signal than vegetation index during the passage of tornado over the region with low vegetation coverage.

The collective spatial pattern in all NSDSIs and the consistent significance suggests the abnormal increase in soil moisture content collocated with the tornado report is not a random phenomenon, thus the underlying mechanism of how tornado passage changes the vertisols reflective properties in SWIR channels deserves further investigation, for example, through another case study when tornadoes occur in right location.

3.2. The Mechanism of Tornado Causing Soil Moisture Scar on Vertisols Cropland

During the tornado passage over homogeneous cropland, some of the topmost soil layer is removed by suction vortices from the tornado, forming surface scars as demonstrated in Figure 1b. After tornado passage, those scars

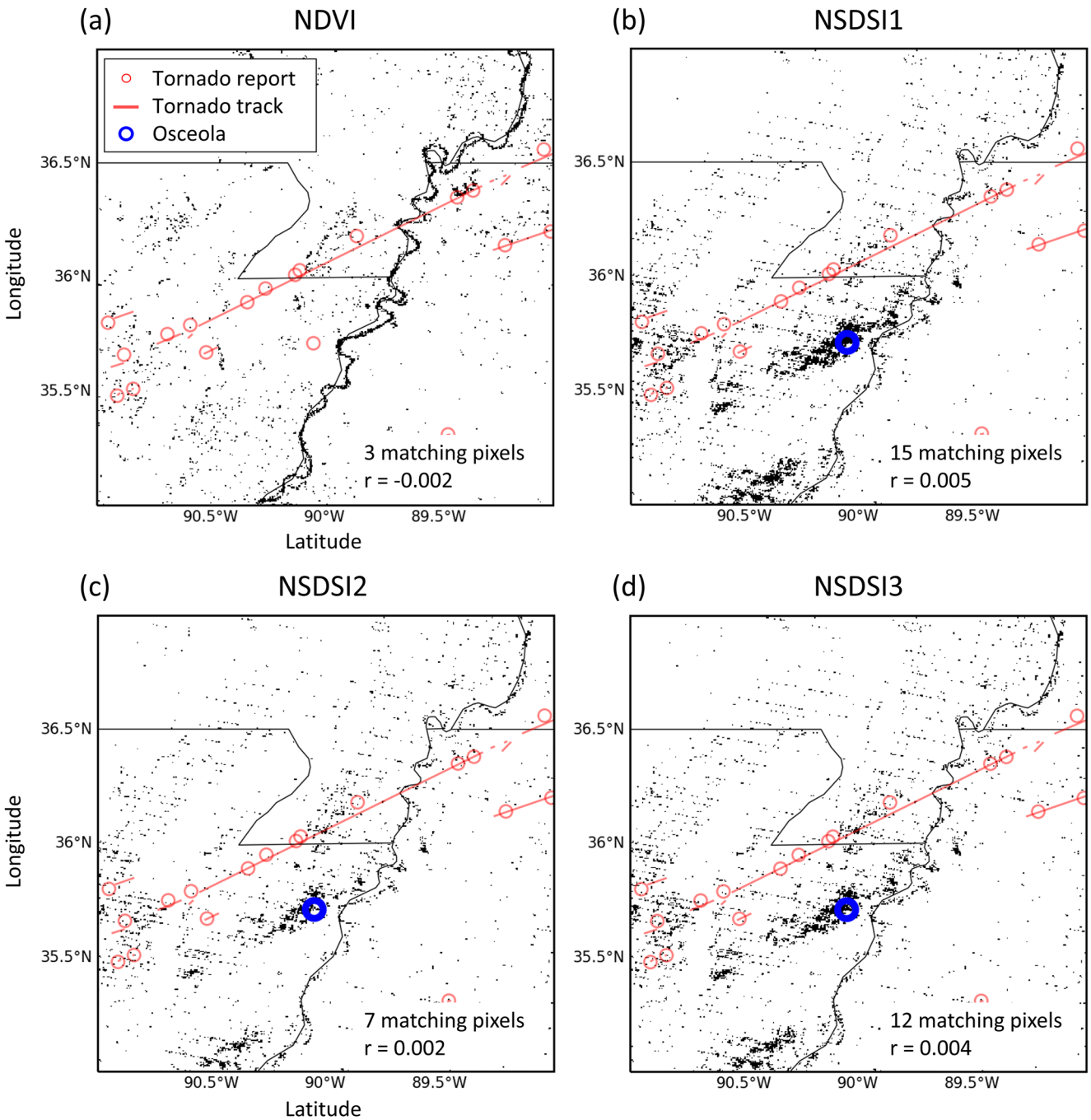

Figure 4. Pixels with the most significant change in (a) NDVI, (b) NSDSI1, (c) NSDSI2, and (d) NSDSI3, overlaid by the tornado reports.

continue to be exposed to wind and precipitation spawned by the tornado-producing supercell and successive systems. However, the recovery rates of those surface scars are different depending on the underlying soil types. For vertisols, although the topmost layer directly exposed to the air is relatively drier because of evaporation, their high plasticity property is still activated because of persistent precipitation. As a result, the surface scars on clayey vertisols can last longer than their counterparts on alfisols, which are relatively sandy and therefore difficult to maintain their shape when exposed to external forcings of wind and precipitation. This only explains why vertisols can better reserve the surface scars for longer time (4 days from 8 December to 12 December), however the significantly higher soil moisture content embedded in those scars is associated with vertisols' vertical moisture profile as illustrated in Figure 5.

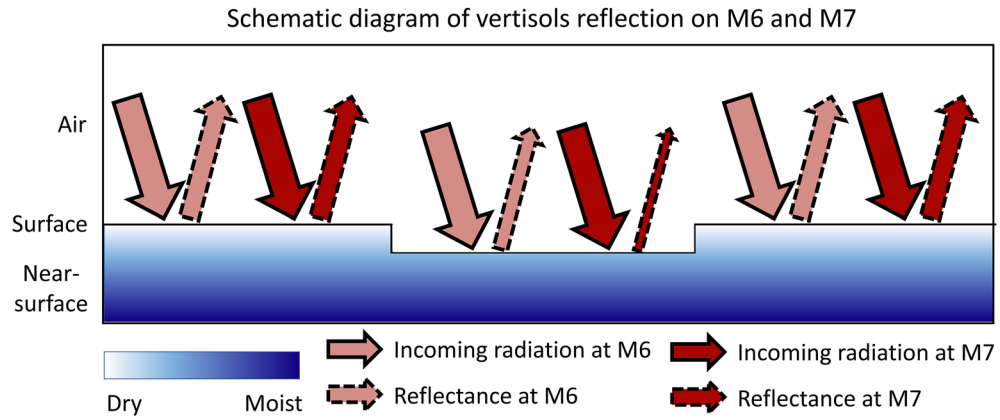

Figure 5. Schematic diagram showing the reflective properties of the scar on vertisols at M6 and M7 channels.

As discussed in Section 2.2, vertisols feature high field capacity, therefore the soil moisture in the near-surface layer is much higher than that in the topmost layer because of the evaporation of the surface moisture. When the topmost soil was removed by tornados' vortices, the underlying soil with higher moisture content was exposed to the air. From Section 2.3, higher soil moisture corresponds to lower SWIR reflectance, but the reduction is more significant in M7 than M6. As a result, the near-surface vertisols with higher soil moisture content are exposed to the air in those scars, causing higher NSDSI signatures. In contrast, although alfisols feature much broader coverage, their capability of retaining surface scars caused by tornado passage is much lower compared to vertisols because of low clay content. Moreover, even those scars were well preserved, the relatively small field capacity of alfisols leads to the small contrast of soil moisture between in the topmost layer and in the near-surface layer, which makes the tornado track signal difficult to detect on SWIR channels.

4. Conclusions and Discussion

This study reveals multiple significant scars with surplus soil moisture over the Arkansas aquert cropland during the 10–11 December 2021 tornado outbreak, one of which is indicative of a tornado track. This is a joint result of (a) the homogeneous cropland with bare soil coverage in winter, (b) the clay-rich vertisols that well retain the structure change caused by tornadoes, and (c) the near-surface soil with higher moisture content being exposed to the air, because the topmost, relatively dry soil is removed by the suction vortices from tornadoes. Consequently, tornado scars on vertisols demonstrate strong signals on SWIR channels, which are further reflected on NSDSIs. In contrast, such signals are difficult to observe over the vast alfisols cropland because of the lower clay content and lower field capacity.

Timely and accurate estimate of tornado touch-down location is critical in severe weather research. Without rich vegetation coverage and high-resolution imagery, the study suggests a quick post-tornado assessment based on MODIS SWIR observations, which feature coarse resolution but a rapid revisit cycle. Therefore, this method is ideal for the examination of winter tornado outbreaks over cropland, where vegetation coverage is low and spotter reports are less reliable because of low population density. In addition to Terra data, the Aqua data of the same day are also examined (Figure S4 in Supporting Information S1). However, the striping noise makes the linear patterns difficult to detect. In addition, MODIS data with longer intervals from 10 to 11 December show weaker signals, which follows the expectation because the disturbed surface recovers with time. Regarding the scars to the bottom of the study domain, they occur over the mixed land use (Figure S1a in Supporting Information S1), therefore the causality of strong signals in NSDSIs warrants further investigation. However, due to the transient nature of tornado outbreaks and the limited access to the sites for field survey, this study lacks direct in-situ soil moisture measurement after tornado passage. Some important measurements, for example, the thickness of removed topmost soil by tornadic suction vortices and the temporal evolution of vertical soil moisture profile after the storms, are not available. As a result, we suggest onsite field observations of soil characteristics should be included in future tornado-related research campaigns like the Verification of the Origins of Rotation in Tornadoes Experiment 2 (VORTEX2; Wurman et al., 2012), as soil could serve as a good medium to record the scale and severity of tornadic vortex.

Finally, it is very important to note that there are numerous clusters of points with significant increase in NSDSIs (Figures 1b and 4) which do not coincide with tornado reports. Spatially, these clusters are located along the eastern border of Arkansas and are exclusively within the domain of vertisols (Figures S1d and S1e in Supporting Information S1). The occurrence of such "null" observations reveals that the high plasticity of the clayey soil not only retains the scars caused by tornadic suction vortices, but also preserves the scratches that result from the removal the topmost soil layer by gusty winds. Moreover, there are a number of other non-meteorological causes that could alter the vertical soil structure like plowing activities. Therefore, caution is needed when applying the soil moisture scar method to identify tornado tracks.

Conflict of Interest

The authors declare no conflicts of interest relevant to this study.

Data Availability Statement

The MODIS data used in this study are downloaded from NASA LAADS DAAC data archive (available at https://ladsweb.modaps.eosdis.nasa.gov/archive/allData/61/MOD02HKM/, last accessed on 1 December 2022). The land use land cover map is obtained from http://soilphysics.okstate.edu/S257/ar/landuse.htm (last accessed on 1 December 2022). The alfisols and vertisols maps are available at https://www.nrcs.usda.gov/conservation-basics/natural-resource-concerns/soils/alfisols (last accessed on 23 January 2023) and https://www.nrcs.usda.gov/conservation-basics/natural-resource-concerns/soils/vertisols (last accessed on 23 January 2023). The datasets for this study are available at https://doi.org/10.5281/zenodo.7648806.

Acknowledgments
This study was supported by the U.S. National Oceanic and Atmospheric Administration (NOAA) grant NA19OAR4310243, the NSF grant AGS-2103820, and the Ministry of Education, Singapore, under its Academic Research Fund Tier 1 (RG74/22 to J. W.). Y. G. acknowledges the support by (while serving at) the National Science Foundation. We would also like to acknowledge high-performance computing support from Cheyenne (https://doi.org/10.5065/D6RX99HX) provided by NCAR's Computational and Information Systems Laboratory, sponsored by the National Science Foundation.

References

Aosier, B., & Kaneko, M. (2007). Evaluation of the forest damage by typhoon using remote sensing technique. In *IEEE international conference on geoscience and remote sensing symposium, IGARSS 2007, Barcelona, Spain, 23–27 July 2007*.

Bell, J. R., & Molthan, A. L. (2016). Evaluation of approaches to identifying hail damage to crop vegetation using satellite imagery. *Journal of Operational Meteorology*, *4*(11), 142–159. https://doi.org/10.15191/nwajom.2016.0411

Changnon, S. A. (2009). Tornado losses in the United States. *Natural Hazards Review*, *10*(4), 145–150. https://doi.org/10.1061/(ASCE)1527-6988(2009)10:4(145)

Chernokulsky, A. V., & Shikhov, A. (2018). 1984 Ivanovo tornado outbreak: Determination of actual tornado tracks with satellite data. *Atmospheric Research*, *207*, 111–121. https://doi.org/10.1016/j.atmosres.2018.02.011

Cho, H. J., Kirui, P., & Natarajan, H. (2008). Test of multi-spectral vegetation index for floating and canopy-forming submerged vegetation. *International Journal of Environmental Research Public Health*, *5*, 477–483. https://doi.org/10.3390/ijerph5050477

Cohen, W. B., & Goward, S. N. (2004). Landsat's role in ecological applications of remote sensing. *BioScience*, *54*(6), 535–545. https://doi.org/10.1641/0006-3568(2004)054[0535:lrieao]2.0.co;2

Coulombe, C. E., Wilding, L. P., & Dixon, J. B. (1996). Overview of Vertisols: Characteristics and impacts on society. *Advances in Agronomy*, *57*, 289–375.

Gallo, K., Smith, T., Jungbluth, K., & Schumacher, P. (2012). Hail swaths observed from satellite data and their relation to radar and surface-based observations: A case study from Iowa in 2009. *Weather and Forecasting*, *27*(3), 796–802. https://doi.org/10.1175/WAF-D-11-00118.1

Han, F. X., Kingery, W. L., Hargreaves, J. E., & Walker, T. W. (2007). Effects of land uses on solid-phase distribution of micronutrients in selected vertisols of the Mississippi River Delta. *Geoderma*, *142*(1–2), 96–103. https://doi.org/10.1016/j.geoderma.2007.08.006

Jedlovec, G. J., Nair, U., & Haines, S. L. (2006). Detection of storm damage tracks with EOS data. *Weather and Forecasting*, *21*(3), 249–267. https://doi.org/10.1175/waf923.1

Kanwar, J. S. (1982). Problems and potentials of Vertisols and Alfisols—The two important soils of SAT—ICRISAT experience. In *Tropical agriculture reearch series No. 5*. DIALOG. Retrieved from http://oar.icrisat.org/4073/1/CP_074.pdf

Kingfield, D. M., & de Beurs, K. M. (2017). Landsat identification of tornado damage by land cover and an evaluation of damage recovery in forests. *Journal of Applied Meteorology and Climatology*, *56*(4), 965–987. https://doi.org/10.1175/JAMC-D-16-0228.1

Klimowski, B. A., Hjelmfelt, M. R., Bunkers, M. J., Sedlacek, D., & Johnson, L. R. (1998). Hailstorm damage observed from the GOES-8 satellite: The 5–6 July 1996 Butte–Meade storm. *Monthly Weather Review*, *126*(3), 831–834. https://doi.org/10.1175/1520-0493(1998)126<0831:HDOFTG>2.0.CO;2

MODIS Characterization Support Team (MCST). (2017). *MODIS 500m calbrated radiance product*. NASA MODIS adaptive processing system. Goddard Space Flight Center. https://doi.org/10.5067/MODIS/MOD02HKM.061

Molthan, A., Jedlovec, G., & Carcione, B. (2011). NASA satellite data assist in tornado damage assessments. *Eos, Transactions American Geophysical Union*, *92*(40), 337–339. https://doi.org/10.1029/2011eo400002

Molthan, A. L., Bell, J. R., Cole, T. A., & Burks, J. E. (2014). Satellite-based identification of tornado damage tracks from the 27 April 2011 severe weather outbreak. *Journal of Operational Meteorology*, *2*(16), 191–208. https://doi.org/10.15191/nwajom.2014.0216

Moriarty, D., Berkowitz, B., & Levitt, Z. (2021). *Deadly path: How tornadoes ripped through states*. The Washington Post. Archived from the original on 11 December 2021.

Pathak, P., Sudi, R., Wani, S. P., & Sahrawat, K. L. (2013a). Hydrological behavior of Alfisols and Vertisols in the semi-arid zone: Implications for soil and water management. *Agricultural Water Management*, *118*(12–21), 12–21. https://doi.org/10.1016/j.agwat.2012.11.012

Pathak, P., Sudi, R., Wani, S. P., & Sahrawat, K. L. (2013b). Hydrological behavior of Alfisols and Vertisols in the semi-arid zone: Implications for soil and water management. *Agricultural Water Management*, *118*, 12–21. https://doi.org/10.1016/j.agwat.2012.11.012

Pettry, D. E., & Switzer, R. E. (1998). Sharkey soils in Mississippi Mississippi agricultural and forestry experiment station. Mississippi State, MS 39762.

Ramsey, E. W., III, Chappell, D. K., & Baldwin, D. G. (1997). AVHRR imagery used to identify hurricane damage in a forest wetland of Louisiana. *Photogrammetric Engineering & Remote Sensing*, *63*, 293–297.

Rouse, J. W., Haas, R. H., Schell, J. A., & Deering, D. W. (1974). Monitoring vegetation systems in the Great Plains with ERTS (Earth Resources Technology Satellite). In *Proceedings of the third Earth resources technology satellite symposium*, (pp. 309–317). NASA GSFC.

Singh, V. P., & Su, Q. (2022). *Irrigation engineering: Principles, processes, procedures, design, and management*. Cambridge University Press.

Skow, K. D., & Cogil, C. (2017). A high-resolution aerial survey and radar analysis of quasi-linear convective system surface vortex damage paths from 31 August 2014. *Weather and Forecasting*, *32*(2), 441–467. https://doi.org/10.1175/WAF-D-16-0136.1

Soil Survey Staff (SSS). (2022). Natural Resources conservation service, United States department of agriculture. Soil Survey Geographic (SSURGO) Database. Retrieved from https://swat.tamu.edu/data/

Szwagrzyk, J., Gazda, A., Doborwolska, D., Checko, E., Zaremba, J., & Tomski, A. (2017). Tree mortality after wind disturbance differs among tree species more than among habitat types in a lowland forest in northeastern Poland. *Forest Ecology and Management*, *398*, 174–184. https://doi.org/10.1016/j.foreco.2017.04.041

Tian, J., Yue, J., Philpot, W. D., Dong, Q., & Tian, Q. (2021). Soil moisture content estimate with drying process segmentation using shortwave infrared bands. *Remote Sensing of Environment*, *263*, 112552. https://doi.org/10.1016/j.rse.2021.112552

Wagner, M., Doe, R. K., Johnson, A., Chen, Z., Das, J., & Cerveny, R. S. (2019). Unpiloted aerial systems (UASs) application for tornado damage survey. *Bulletin of the American Meteorological Society*, *100*(12), 2405–2409. https://doi.org/10.1175/BAMS-D-19-0124.1

Wang, W., Qu, J. J., Hao, X., Liu, Y., & Stanturf, J. A. (2010). Post-hurricane forest damage assessment using satellite remote sensing. *Agricultural and Forest Meteorology*, *150*(1), 122–132. https://doi.org/10.1016/j.agrformet.2009.09.009

Wurman, J., Dowell, D., Richardson, Y., Markowski, P., Rasmussen, E., Burgess, D., et al. (2012). The second verification of the origins of rotation in tornadoes experiment: VORTEX2. *Bulletin of the American Meteorological Society*, *93*(8), 1147–1170. https://doi.org/10.1175/BAMS-D-11-00010.1

Yuan, M., Dickens-Micozzi, M., & Magsig, M. A. (2002). Analysis of tornado damage tracks from the 3 May tornado outbreak using multispectral satellite imagery. *Weather and Forecasting*, *17*, 382–398. https://doi.org/10.1175/1520-0434(2002)017<0382:AOTDTF>2.0.CO;2

Yue, J., Tian, J., Tian, Q., Xu, K., & Xu, N. (2019). Development of soil moisture indices from differences in water absorption between shortwave-infrared bands. *ISPRS Journal of Photogrammetry and Remote Sensing*, *154*, 216–230. https://doi.org/10.1016/j.isprsjprs.2019.06.012